Photoionization of the outer shells of neon, argon, krypton, and xenon using the relativistic random-phase approximation

W. R. Johnson
Department of Physics, University of Notre Dame, Notre Dame, Indiana 46556

K. T. Cheng
Argonne National Laboratory, Argonne, Illinois 60439

(Received 18 January 1979)

Multichannel photoionization calculations using the relativistic random-phase approximation for the outer shells in the rare gases, neon, argon, krypton, and xenon, are presented. Total cross sections and partial cross sections for ns subshells are determined and compared with experiment and with alternative calculations at low energies. Branching ratios of $^2P_{3/2}$:$^2P_{1/2}$ cross sections which are sensitive to relativistic and correlation effects are presented and compared with experiment. Angular distribution asymmetry parameters β determined for each subshell are found and compared with experiment; the differences between β values for $^2P_{1/2}$ and $^2P_{3/2}$ subshells in krypton and xenon emphasize the importance of relativistic effects in outer subshells of heavy elements. Values of β are given for outermost s electrons which show large relativistic effects near the "Cooper minima" of the corresponding partial cross sections. Eigenphases from the multichannel analysis are presented for argon to illustrate mathematical features of the present calculation.

I. INTRODUCTION

Electron correlations are known to be significant in the photoionization process,[1,2] and those correlations most important in low-energy photoionization are accurately accounted for by the random-phase approximation.[3,4] Incorporating relativity into the random-phase approximation enables us to describe refined details of atomic photoionization such as individual subshell angular distributions[5] and partial cross-section branching ratios[6] for which relativistic fine-structure effects play a prominent role. It is the purpose of this paper to illustrate the interplay between correlations and relativity in low-energy photoionization as it appears in the theoretical studies of rare gases using the relativistic random-phase approximation (RRPA).

In a previous paper[7] (which we shall refer to as I in the sequel) we have shown in elaborate detail how the RRPA is applied to analyze multichannel photoionization. Specifically, we explained how the RRPA photoionization amplitudes and cross sections are obtained in terms of single-particle orbitals which satisfy radial RRPA equations, and we described how multichannel solutions of the radial RRPA equations are obtained.

In the present discussions we will be concerned mainly with low-energy photoionization processes where photon energies are less than 150 eV, so that we may restrict our attention to dipole contributions to the photoionization amplitude. In the dipole approximation the photoionization differential cross section for each subshell is given by I, Eq. (56):

$$\frac{d\sigma_{n\kappa}}{d\Omega} = \frac{\sigma_{n\kappa}(\omega)}{4\pi}\left[1 - \tfrac{1}{2}\beta_{n\kappa}(\omega)P_2(\cos\theta)\right]. \tag{1}$$

The subscripts n, κ are the principal and angular momentum quantum numbers ($\kappa = -1, 1, -2, 2, \ldots$ describes the sequence $s_{1/2}, p_{1/2}, p_{3/2}, d_{3/2}, \ldots$); $\sigma_{n\kappa}(\omega)$ is the subshell cross section and $\beta_{n\kappa}(\omega)$ is the angular distribution asymmetry parameter. The angle θ in Eq. (1) is measured between the directions of the incident photon and the photoelectron, and ω is the photon energy.

We have carried out numerical RRPA calculations of $\sigma_{n\kappa}(\omega)$ and $\beta_{n\kappa}(\omega)$ for the outer $np_{3/2}$, $np_{1/2}$, and $ns_{1/2}$ subshells of the rare gases Ne, Ar, Kr, and Xe at low energies, and, in the body of this paper, we present these calculations and compare them with other related theoretical and experimental studies. Generally, we find that relativistic effects in Ne and Ar are small so that the RRPA studies agree well with the nonrelativistic random-phase approximation (RPAE) of Amusia and coworkers[3] and with other many-body calculations such as the many-body perturbation theory (MBPT) of Kelly and Simons[8] or of Chang,[9,10] and the R-matrix theory of Burke and Taylor.[11] For Kr relativistic effects on cross-section branching ratios and asymmetry parameters are significant and the importance of a relativistic treatment becomes

apparent. The branching ratios and asymmetry parameters for Xe show large relativistic effects; however, relativistic considerations alone do not suffice to explain quantitatively the experimental data, since careful consideration must be given to correlation effects also.[5,6] We describe our results on total cross sections, partial cross sections, branching ratios, and angular distributions in Secs. II–V. In Sec. VI we comment on details of the final-state electron-ion interaction, and in the Appendix we outline our procedure for solving the RRPA equations using radial Green's functions.

II. TOTAL CROSS SECTIONS

The results of the truncated RRPA calculations for the total photoionization cross sections for Ne, Ar, Kr, and Xe are shown in Figs. 1–4, respectively. One general observation that can be made from these figures is that correlation effects as measured by the difference between Hartree-Fock[12] (HF) and RRPA is sizable in all four of the rare gases considered; moreover, it is apparent that the correlated RRPA calculations are in significantly better agreement with experiments (Marr and West,[13] West and Morton,[14] Samson,[15] Watson[16]) than the corresponding HF values. Indeed, the difference between HF length form calculations (HF $-L$) and HF velocity form calculations (HF $-V$) is often larger than the difference between either HF calculation and experiment! By contrast, the RRPA length and velocity results agree to within a few percent throughout this entire calculation. It should be mentioned that the present

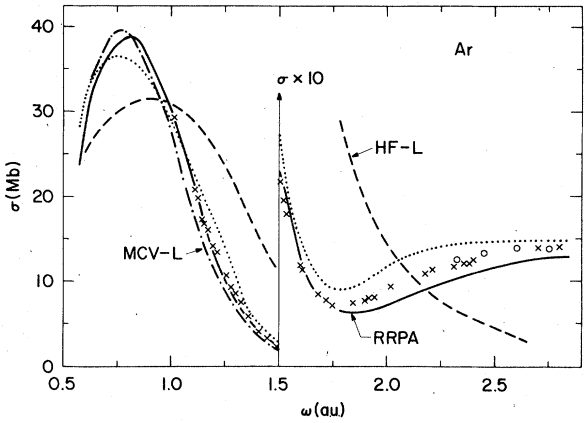

FIG. 2. Photoionization cross sections for argon as functions of photon energy ω. Experiment: ····· Marr and West, Ref. 13; × Samson, Ref. 15; O Watson, Ref. 16. Theory: — this work; —·— Swanson and Armstrong, Ref. 17; — — — Kennedy and Manson, Ref. 12.

RRPA results are generally in close agreement with the nonrelativistic RPAE, as well as with other many-body calculations.[3,8,9,11,17] A typical comparison between the RRPA and another many-body calculation is given in Ar (Fig. 2) where we plot the length form results of the multiconfiguration $V^{(N-1)LS}$ (MCV-L) calculation by Swanson and Armstrong,[17] together with the RRPA and with experiments. In Ne we call attention to the relativistic R-matrix calculation of Chang,[18] which also agrees well with its nonrelativistic counterpart. These agreements are not particularly surprising since relativistic effects are expected to be small

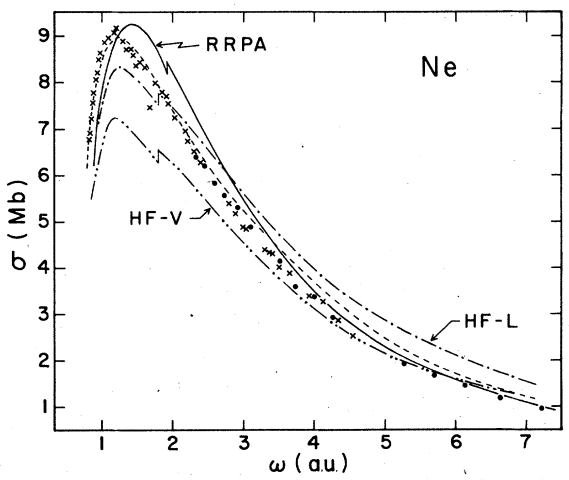

FIG. 1. Photoionization cross sections for neon as functions of photon energe ω. Experiment: ---- Marr and West, Ref. 13; × Samson, Ref. 15; ● Watson, Ref. 16. Theory: —— this work; —·— and —··— Kennedy and Manson, Ref. 12, HF length and velocity form results, respectively.

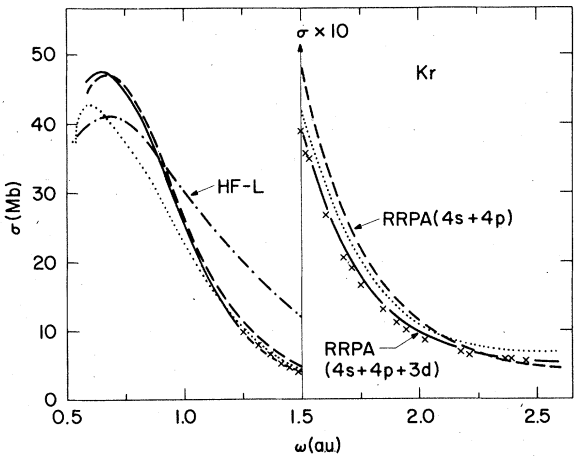

FIG. 3. Photoionization cross sections for krypton as functions of photon energy ω. Experiment: ····· Marr and West, Ref. 13; × Samson, Ref. 15. Theory: —— and ---- this work, three- and two-shell correlation results, respectively; —·— Kennedy and Manson, Ref. 12.

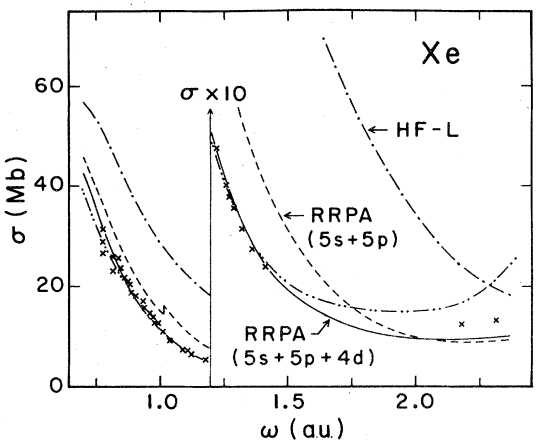

FIG. 4. Photoionization cross sections for xenon as functions of photon energy ω. Experiment: —••— West and Morton, Ref. 14; ×Samson, Ref. 15. Theory: —— and ---- this work, three- and two-shell correlation results, respectively; —•—Kennedy and Manson, Ref. 12.

for light elements and for outer shells in heavy elements.

In the present calculations for Ne and Ar in Figs. 1 and 2, we have included two-shell correlations between the valence np shell and the neighboring ns shell. The resulting two-shell correlation calculation involves seven interacting channels, viz.,

$$ns_{1/2} \rightarrow p_{1/2}, \quad ns_{1/2} \rightarrow p_{3/2},$$
$$np_{1/2} \rightarrow s_{1/2}, \quad np_{1/2} \rightarrow d_{3/2},$$
$$np_{3/2} \rightarrow s_{1/2}, \quad np_{3/2} \rightarrow d_{3/2}, \quad np_{3/2} \rightarrow d_{5/2}.$$

Below the $ns_{1/2}$ threshold our calculation includes five open channels and two closed channels, while above the threshold all seven channels are open.

The total cross sections in Ne and Ar are insensitive to the intershell correlation between ns and np. However, because of the coupling between closed $ns \rightarrow p$ channels and the open $np \rightarrow s, d$ channels, a series of autoionizing resonances occurs below the ns threshold.[19] In principle, our seven channel calculations are capable of studying these resonance phenomena. As a matter of fact, the inner ns shell autoionizing resonances in rare gases have been studied with the nonrelativistic RPAE.[3] However, since we are using an iterative scheme in solving the RRPA equations, the convergence of the RRPA solutions near these resonances usually causes numerical difficulties. We believe that a more practical way of studying autoionizing resonances is to apply the multichannel quantum defect theory[20] in analyzing phase-shift data obtained from the RRPA, but that is outside the scope of this work. For our present purposes, we avoid these resonances altogether and give only the smooth background cross section. Similar resonances should also show up in RRPA calculations in the gap between the $np_{1/2}$ and $np_{3/2}$ thresholds for the rare gases.

In Kr and Xe it has been established that correlation between outer np and ns shells and the inner $(n-1)d$ shell alters the total cross section.[3] We present results from our RRPA calculations with and without $(n-1)d$ correlations in Figs. 3 and 4. It can be seen that inclusion of the $(n-1)d$ shell correlations improves the agreement of the RRPA calculations with experiment substantially for both Kr and Xe. Including the $(n-1)d$ shell in the calculation increases the number of channels to be treated from 7 to 13, since we must consider the channels

$$nd_{3/2} \rightarrow p_{1/2}, \quad nd_{3/2} \rightarrow p_{3/2}, \quad nd_{3/2} \rightarrow f_{5/2},$$
$$nd_{5/2} \rightarrow p_{3/2}, \quad nd_{5/2} \rightarrow f_{5/2}, \quad nd_{5/2} \rightarrow f_{7/2},$$

in addition to those already considered for two-shell correlation calculations. We note by comparing Fig. 3 with Fig. 4 that the $4d$ shell is much more important for Xe than the corresponding $3d$ shell is for Kr.

Figures 1–3 show further that there are larger discrepancies between RRPA and experiment near threshold than elsewhere. These large threshold effects can be traced to the strong correlation between the low-energy photoelectron and the residual ion which are not accounted for properly by the RPA technique. Extensions of the RPA to include "relaxation" effects at low energies have improved the agreement in the nonrelativistic case[3] and presumably would have the same effect relativistically. In fact, we see that the agreement between theory and experiment improves with increasing energy in all cases considered with the possible exception of Xe at photon energies between 2.2 and 2.5 a.u.; however, at these energies there remains a substantial disparity between different experimental determinations of the Xe cross section.[14,15]

In summary, we find close agreement between the present RRPA calculations of total cross sections and the RPAE calculations of Amusia and Cherepkov.[3] The correlation effects are seen to be much more important than relativistic effects for total cross sections, and inclusion of correlations using RPA methods brings theoretical predictions into agreement with experiment except at threshold where relaxation effects become important. Although no significant relativistic effects show up in the total cross sections, we do expect and find interesting relativistic effects in partial cross sections, branching ratios, and an-

gular distributions which are to be discussed in the following sections.

III. PARTIAL CROSS SECTIONS FOR *ns* SUBSHELLS

Decomposing the total cross section for rare gases into partial cross sections from individual subshells provides more detailed information on the dynamics of the photoionization process. Partial cross sections are experimentally determined by measuring the ratio of intensities of individual lines in the photoelectron spectra and normalizing to the observed total cross sections.[1] Since the total cross sections (which are dominated by the $np \rightarrow d$ transition at the energies considered) are presently determined to between 3% and 10% accuracy,[1] the partial cross sections are necessarily less accurate. Nevertheless, more and more data[21] are being accumulated on inner-shell $ns \rightarrow p$ transitions so that meaningful comparisons between theory and experiment are now possible.

In Figs. 5–8 these inner $ns \rightarrow p$ cross sections are plotted against photon energy. The experimental cross sections, except for Ne, decrease from threshold and pass through a "Cooper minimum" near $\omega \simeq 1.4$ a.u. As seen from these figures, the RRPA, along with other many-body theories, reproduces this behavior, giving a "Cooper minimum" at approximately the correct photon energy for Ar, Kr, and Xe, but no minimum for Ne. The existence of such a minimum above the *ns* threshold is a fine example of a correlation effect which

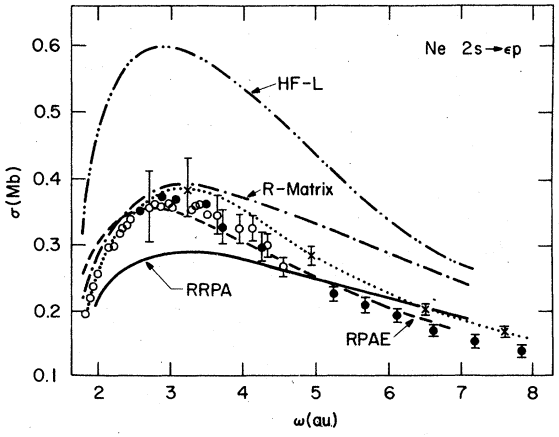

FIG. 5. Partial photoionization cross sections for the 2*s* subshell of neon as functions of photon energy ω. Experimental data are obtianed from Wuilleumier and Krause (Ref. 22) scaled by total cross sections from Marr and West •••⧖••• (Ref. 13), from Samson ⧖ (Ref. 15), and from Watson ⧗ (Ref. 16). Theory: —this work; ---- Amusia *et al.*, Ref. 3; -•- Burke and Taylor, Ref. 11; -•••- Kennedy and Manson, Ref. 12.

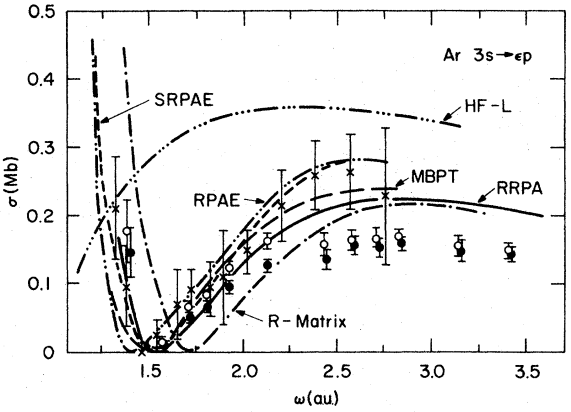

FIG. 6. Partial photoionization cross sections for 3*s* subshell of argon as functions of photon energy ω. Experiment: ⧖ Tan and Brion, Ref. 24; ⧖ and ⧗, Adam *et al.*, Ref. 25 (scaled by total cross sections from Marr and West, Ref. 13, and from Samson, Ref. 15, respectively). Theory: —this work; —••— Amusia *et al.*, Ref. 3; --- Simplified RPAE of Lin, Ref. 23; — — Chang, Ref. 10; —•— Burke and Taylor, Ref. 11; —•••—Kennedy and Manson, Ref. 12.

is not properly described by HF calculations.

In Ne, the present RRPA calculations are seen to be smaller than other theoretical many-body results[3,11] near threshold. The discrepancy between the present calculation and the RPAE is probably not due to any intrinsic physical reason, since relativistic effects are negligible for the 2*s* shell in Ne. Furthermore, no such disagreement exists for the Ne 2*p* cross sections. Thus we believe that the discrepancy here is probably a re-

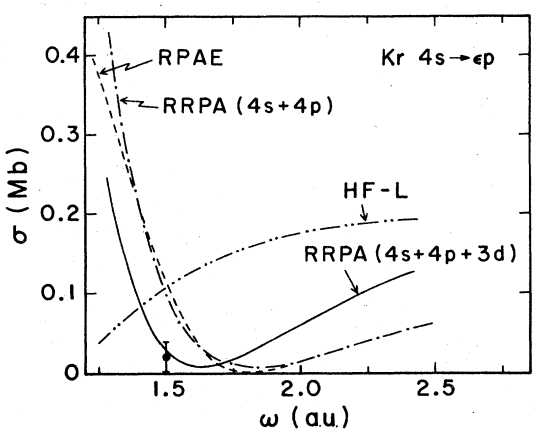

FIG. 7. Partial photoionization cross sections for the 4*s* subshell of krypton as functions of photon energy ω. Experiment: ⧗ Samson and Gardner, Ref. 26. Theory: — and —•— this work, three- and two-shell correlation results, respectively; ---- Amusia *et al.*, Ref. 3; —••—Kennedy and Manson, Ref. 12.

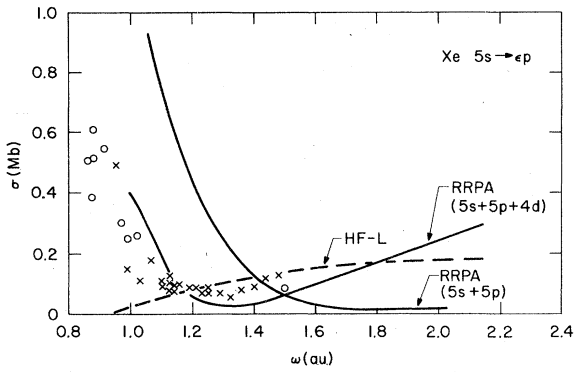

FIG. 8. Partial photoionization cross sections for the 5*s* subshell of xenon as functions of photon energy ω. Experiment: O Samson and Gardner, Ref. 26; × Gustafsson, Ref. 27. Theory: —— this work; ---- Kennedy and Manson, Ref. 12.

sult of different numerical techniques employed. In any case, the disagreement with RPAE and with experiment[22] diminishes as photon energy increases.

We compare various theoretical[3,10-12,23] and experimental[24,25] values for the Ar $3s \rightarrow p$ cross section in Fig. 6. The position of the "Cooper minimum" predicted by various theoretical methods (with the exception of the uncorrelated HF calculation) all appear to agree with one another and with experiment to within a few eV. The disparity between RRPA and RPAE is due, in this case, to the use of the experimental threshold in RPAE and the theoretical thresholds in RRPA, and should not be construed as a relativistic effect.

In Figs. 7 and 8, we show comparisons between theory[3,12] and experiment[26,27] for the 4*s* and 5*s* cross sections in Kr and Xe, respectively. One interesting observation is the influence of correlation with the inner $(n-1)d$ shells on the location of the "Cooper minima" for the ns cross sections. As can be seen from the figures, the inner $(n-1)d$ shell shifts the minimum by $\simeq 10$ eV and reduces its width. While relatively few experimental data are available for the 4*s* and 5*s* subshells of Kr and Xe, the three-shell correlation calculations appear to agree better with available data than do the two-shell calculations omitting the $(n-1)d$ shell correlations.

One other interesting point is that, according to the single-particle theory,[28] the cross section vanishes at a "Cooper minimum" where the amplitude passes through zero. Because of interchannel coupling, nonrelativistic many-body calculations give nonzero but very small amplitudes at "Cooper minima." Relativistically,[29] the amplitudes for $ns \rightarrow p_{1/2}$ and $ns \rightarrow p_{3/2}$ vanish at slightly different energies, so even in the absence of interchannel coupling, relativistic effects dominate near a "Cooper minimum" and give much larger cross sections than predicted nonrelativistically. The size of the 5*s* cross section of Xe near $\omega = 1.3$ a.u. is a case in point. One sees from Fig. 8 that the experimental values of the cross section near the "Cooper minimum" are in good agreement with relativistic calculations, but they are found to be much larger than nonrelativistic predictions. Later we will see that the size of the amplitude at the "Cooper minimum" influences the corresponding angular distribution.

IV. PARTIAL CROSS-SECTION BRANCHING RATIOS

Since the nonrelativistic Schrödinger Hamiltonian is independent of spin, the cross section per electron from two subshells with the same orbital angular momentum but different total angular momenta will be identical. It follows that the partial cross-section branching ratio for two such subshells will be the "statistical ratio" given by their relative occupation, to the extent that spin-orbit and other relativistic effects can be neglected. Experimentally,[30] it has been known for some time that the branching ratios of outer np cross sections for the rare gases depart from the statistical ratio of 2, and it is found that the measured ratio provides an interesting and exacting test of relativistic theories.

For Ne, the RRPA predicts that the $2p_{3/2}:2p_{1/2}$ branching ratio remains within 1% of the statistical value of 2 over the entire range of energies considered in the present calculation, in harmony with nonrelativistic expectations. The situation for Ar illustrated in Fig. 9 is somewhat more interesting. Near threshold, the calculated ratio is slightly smaller than the statistical ratio of 2 and is consistent with the measured value of 1.93.[30] As the photon energy increases beyond the "Cooper minimum" near $\omega = 1.7$ a.u. the ratio increases sharply to about 2.1 and then decreases gradually toward the statistical value. The sharp increase is due to the fact that the $p_{3/2}$ cross section reaches its minimum at lower energy than the $p_{1/2}$ cross section and starts increasing, while the $p_{1/2}$ cross section is at a relatively low value.[29] The similar behavior for Kr is also illustrated in Fig. 9. Near the threshold the branching ratio is consistent with the experimental value 1.77,[30] while at higher energies the ratio increases sharply as the $p_{3/2}$ cross section, and later the $p_{1/2}$ cross section, pass through their respective "Cooper minima." When three-shell correlations are included in the RRPA calculations the "Cooper minima" are shifted to lower energy and the point at which the branching

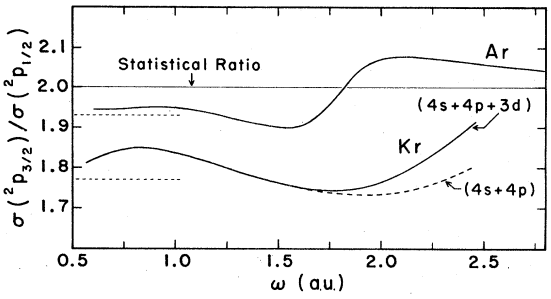

FIG. 9. $^2P_{3/2}$: $^2P_{1/2}$ branching ratios for argon and krypton as functions of photon energy ω. The short dashed lines are the experimental values of Samson *et al.*, (Ref. 30) at low energy.

ratio starts to increase above 2 is correspondingly shifted, as shown in the figure.

We compare our calculated branching ratio for Xe with experimental measurements[31] and with relativistic Dirac-Slater (DS)[31] and Dirac-Fock (DF)[32] calculations in Fig. 10. The RRPA is seen to represent the experimental values better than the uncorrelated relativistic calculations. The RRPA calculations, including three-shell correlations, increase from well below the statistical ratio of 2 near threshold to above 2 near $\omega = 2.3$ a.u. in good agreement with experiment, while the two-shell correlation calculation predicts a rise at a higher photon energy.

Because of the sensitivity of the branching ratio to details of the electron correlations, such measurements provide interesting tests of relativistic and correlation effects in the photoionization process.

V. ANGULAR DISTRIBUTION ASYMMETRY PARAMETERS

Our values for the angular distribution asymmetry parameters β for the np shells are given in Figs. 11–14. For Ne and Ar, the RRPA predicts values of $\beta(np_{1/2})$ and $\beta(np_{3/2})$ in very close agreement since relativistic effects are small. In Figs. 11 and 12, we plot the average values

$$\beta_{np} = \frac{\beta_{np_{1/2}}\sigma_{np_{1/2}} + \beta_{np_{3/2}}\sigma_{np_{3/2}}}{\sigma_{np_{1/2}} + \sigma_{np_{3/2}}} \tag{2}$$

against photon energy. We see that the RRPA predictions agree well with R-matrix[33] values, as well as with experimental[34–37] determinations; the RRPA also agrees very well with the RPAE values which are not shown in these graphs.

Relativistic effects are already apparent for the $4p$ angular distribution parameters in Kr shown in Fig. 13, where we plot our calculations, including three-shell correlations, together with experiments.[35,38] Only the weighted average of our two-shell values are given; these two-shell values are included to illustrate once again the importance of correlations with the inner $(n-1)d$ shell, especially near the "Cooper minimum." Our results, including three-shell correlations, are given in a more detailed way by plotting the individual subshell β parameters against photon energy. Near threshold, the relativistic theory gives values of $\beta(4p_{3/2})$ which are larger than $\beta(4p_{1/2})$, in good agreement with the experimental determination. The RRPA calculations predict that the ordering of the β parameters will be reversed $[\beta(4p_{1/2}) > \beta(4p_{3/2})]$ for photon energies above 1.6 a.u. where, unfortunately, only weighted average experimental values are presently available.

The more dramatic relativistic effects occurring

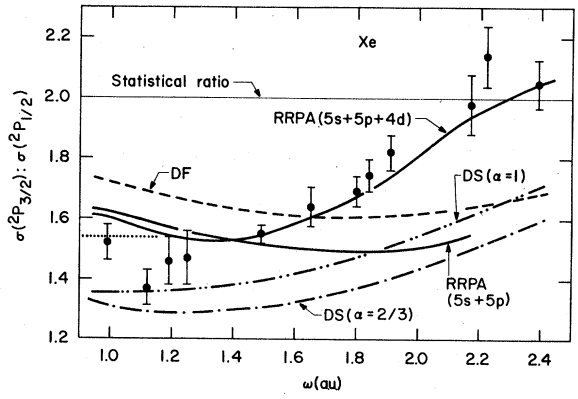

FIG. 10. $^2P_{3/2}$: $^2P_{1/2}$ branching ratio for xenon as a function of photon energy ω. Experiment: •••• Samson *et al.*, Ref. 30; ⧳ Wuilleumier *et al.*, Ref. 31. Theory: — this work; --- Ong and Manson, Ref. 32; —•—and —••— Wuilleumier *et al.*, Ref. 31.

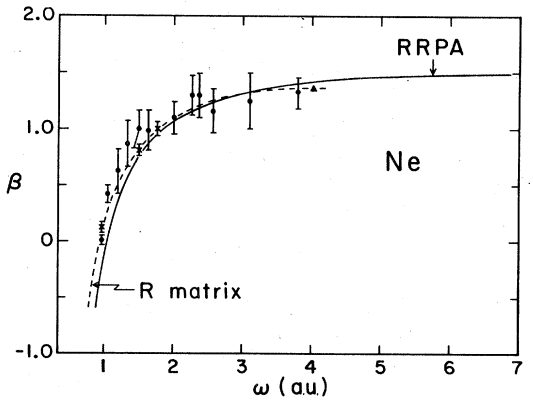

FIG. 11. Averaged asymmetry parameter β for the $2p$ shell of neon as a function of photon energy ω. Experiment: ⧳ Codling *et al.*, Ref. 34; ⧲ Dehmer *et al.*, Ref. 35; ▲ Wuilleumier and Krause, Ref. 36. Theory: — this work; ---- Taylor, Ref. 33.

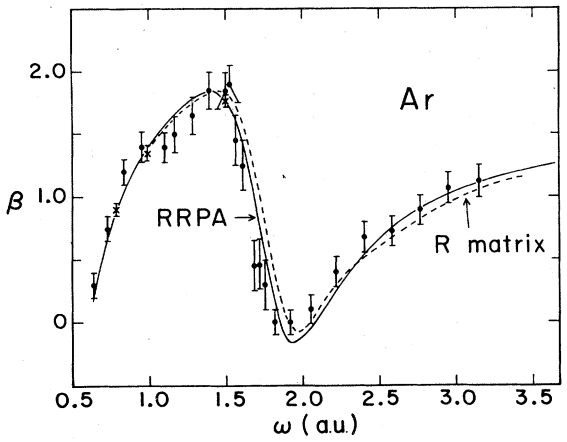

FIG. 12. Averaged asymmetry parameter β for the $3p$ shell of argon as a function of photon energy ω. Experiment: ⧳ Houlgate *et al.*, Ref. 37; ⧖ Dehmer *et al.*, Ref. 35. Theory: — this work; ---- Taylor, Ref. 33.

in Xe are shown in Fig. 14, where we plot the individual curves for $\beta(5p_{3/2})$ and $\beta(5p_{1/2})$ using our three-shell correlation calculation against photon energy. The ordering is similar to that predicted for Kr, with $\beta(5p_{3/2})$ larger than $\beta(5p_{1/2})$ near threshold and $\beta(5p_{1/2})$ larger than $\beta(5p_{3/2})$ beyond $\simeq 1.2$ a.u. Experimental measurements[35] exist both above and below the crossing point confirming the predicted ordering. Moreover, the measured

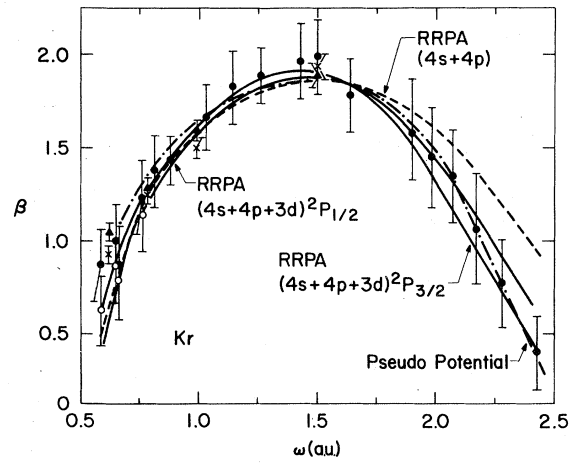

FIG. 13. Asymmetry parameters β for the $4p$ shell of krypton as functions of photon energy ω. Experiment: ⧳ and ⧗ Miller *et al.*, Ref. 38, for $\beta(^2P_{3/2})$ and $\beta(^2P_{1/2})$, respectively (when there is no distinction between subshell β parameters ⧳ represents the common measured value); ▲ and ⧖, Dehmer *et al.*, Ref. 35, for $\beta(^2P_{3/2})$ and $\beta(^2P_{1/2})$, respectively. Theory: — this work; ---- the averaged β values of this work from a two-shell correlation calculation; —·— Miller *et al.*, Ref. 38.

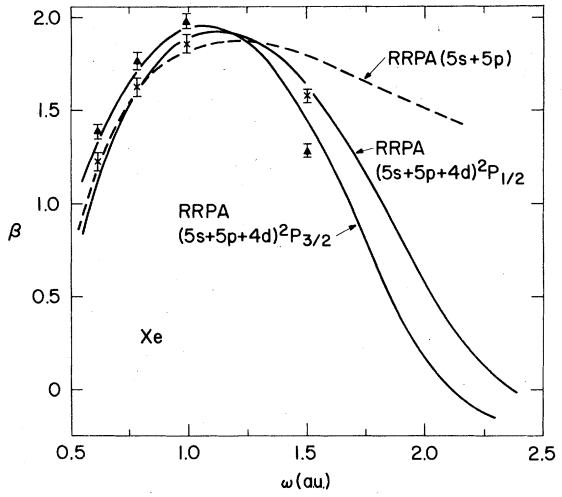

FIG. 14. Asymmetry parameters β for the $5p$ shell of xenon as functions of photon energy ω. Experiment: ▲ and ⧖, Dehmer *et al.*, Ref. 35, for $\beta(^2P_{3/2})$ and $\beta(^2P_{1/2})$, respectively. Theory: — this work; --- the averaged β values of this work from a two-shell correlation calculation.

values are in close agreement with the RRPA predictions. By contrast, the RRPA calculations with two-shell correlations which are also shown in Fig. 14, disagree significantly with experiment, especially at higher energies toward the "Cooper minimum."

Even more dramatic are the relativistic effects on the ns shells of the rare gases which are illustrated in Fig. 15. Nonrelativistically, the angular distribution parameter β_{ns} has the value[28]

$$\beta_{ns}^{\mathrm{NR}} = 2\,, \tag{3}$$

independent of energy for all of the cases illustrated in Fig. 15. Relativistically, the expression for β_{ns} is modified to[5]

$$\beta_{ns} = 2 - \frac{3|A_T|^2}{|A_S|^2 + |A_T|^2}\,, \tag{4}$$

where A_S and A_T are amplitudes for exciting singlet and triplet final states. The amplitude A_T is assumed to vanish in nonrelativistic calculations, so that Eq. (4) reduced to Eq. (3). As can be seen from Eq. (4), the effects of a nonzero value of A_T will be amplified near the "Cooper minimum" where A_S is small. Indeed, if we assume that A_S vanishes at the "Cooper minimum," then we find $\beta_{ns} = -1$. In our relativistic calculations, we include both A_S and A_T; since A_S is small but nonvanishing at the "Cooper minimum," we find that β_{ns} departs from the nonrelativistic value of 2, but never decreases to the limiting value of -1. Our results for Ar in Fig. 15 show a small departure

from $\beta = 2$ very near the $3s$ "Cooper minimum," which will be difficult to verify experimentally because of the smallness of the cross section. For Kr, the size of the relativistic effect is enhanced because the relative size of A_T/A_S near the "Cooper minimum" is increased. Finally, for Xe, the RRPA predicts a very large relativistic effect near the "Cooper minimum." For Kr and Xe, we give both the two-shell correlation results and the three-shell results, although it should be clear that the three-shell calculations are to be preferred. Several alternative calculations are also given for Xe; one by Walker and Waber[29] illustrates the dependence of β on photon energy in an uncorrelated DS calculation, another calculation of β by Huang and Starace[39] includes the spin-orbit interaction in a nonrelativistic K-matrix theory, and a third calculation by Cherepkov[40] is based on the nonrelativistic RPAE. Presently, only a single datum[41] exists at $\omega = 1.5$ a.u. and further experimental values would certainly provide valuable tests of the interplay between correlation and relativity mentioned in the Introduction.

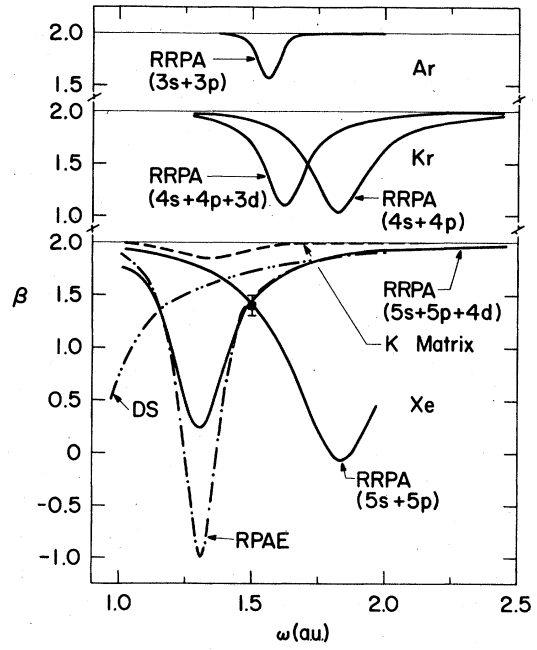

FIG. 15. Asymmetry parameters β for the outermost ns shells of argon, krypton, and xenon as functions of photon energy ω. Experiment: ⊢ Dehmer and Dill, Ref. 41. Theory: — this work; ---- Huang and Starace, Ref. 39; —·— Cherepkov, Ref. 40; —··— Walker and Waber, Ref. 29.

VI. FINAL-STATE ELECTRON-ION INTERACTION

In the course of solving the RRPA equations, we obtain detailed information about the interaction of the outgoing photoelectron and the residual ion. As a preliminary step in our analysis, we obtain solutions to the RRPA equations satisfying convenient mathematical boundary conditions from which we may construct a K matrix,[42] as described in the Appendix. With the aid of the K matrix, we obtain a family of eigenchannel solutions to the RRPA equations; these are linear combinations of the preliminary solutions which diagonalize the K matrix. The eigenchannel solutions are used, in turn, to determine "physical" solutions satisfying outgoing wave boundary conditions, which require an outgoing wave in one channel and incoming waves in all other channels.

Each eigenvalue λ_α of the K-matrix is related to an eigenphase $\delta_\alpha(\omega)$, which describes the common phase displacement of the orbitals in an eigenchannel by

$$\lambda_\alpha = \tan\delta_\alpha . \tag{5}$$

Since we base our K matrix on Dirac-Coulomb orbitals, the corresponding phase shifts relfect only the short-range parts of the electron-ion interactions,[43] and are therefore related to eigenchannel quantum defects.[44]

To illustrate some results from our analysis, we consider the case of Ar in Fig. 16, where we plot the eigenphases for the $(J^\pi = 1^-)$ electron-ion interaction as it is obtained from the two-shell $(3s + 3p)$ correlation solution to the RRPA equations. Near threshold, we have five open channels and correspondingly five eigenchannels, while beyond the $3s$ threshold we have seven open channels and seven eigenchannels. Since relativistic effects

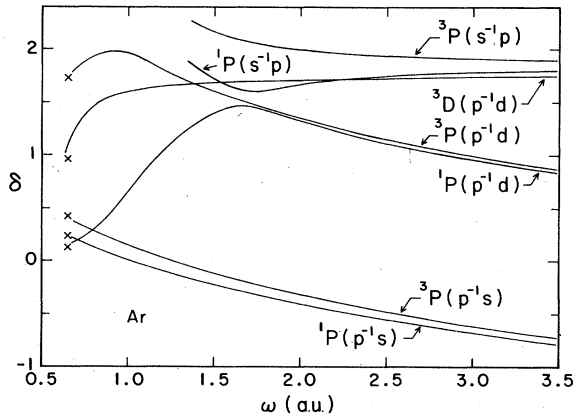

FIG. 16. Eigenphases of the photoelectron in argon as functions of photon energy ω. The crosses are semiempirical values obtained from the multichannel quantum defect analysis of Lee, Ref. 43.

are small in Ar, we find that the eigenchannels are almost pure LS states. Very near threshold we find that the eigenchannels further reduce to single-configuration LS states, and we take advantage of that circumstance to label the eigenchannels in Fig. 16 by the corresponding configurations. As energy increases above the threshold, the eigenchannels retain their LS character, except near the crossing points of the singlet and triplet eigenphases. Because of the strong interaction between the $P(s^{-1}p)$ and $P(p^{-1}d)$ channels near $\omega = 1.5$ a.u. the configurations contributing to these two eigenchannels are in fact interchanged at higher energies so that the curves labeled by $P(s^{-1}p)$ are mainly of $(p^{-1}d)$ character, and those labeled by $P(p^{-1}d)$ are mainly $(s^{-1}p)$.

The excitation amplitude may be decomposed into eigenchannels along with the orbitals. For Ar, we find that the excitation amplitude is dominated by the $^1P(p^{-1}d)$ eigenchannel near threshold, that the $^1P(p^{-1}s)$ eigenamplitude is small, and that the remaining triplet amplitudes are negligible. For the other rare gases the situation is similar, and for Kr and Xe the triplet amplitudes play an important role near the "Cooper minima," as has been stressed in the previous sections.

ACKNOWLEDGMENTS

The authors are grateful to Dr. J. A. R. Samson, Dr. F. Wuilleumier, Dr. J. B. West, and Dr. K. N. Huang for communicating their results prior to publication. We also thank Dr. C. M. Lee, Dr. C. D. Lin, and Dr. J. L. Dehmer for helpful discussions. One of us (W.R.J.) thanks the Argonne University Association for a Faculty Research Participant appointment. This work was performed in part under the auspices of the U. S. Department of Energy and was supported in part by NSF Grant No. PHY-77-15141.

APPENDIX

As a practical matter in solving the RRPA equations for closed-shell atoms, we restrict our attention to a few subshells which interact significantly and we deal with the resulting truncated RRPA equations. Let us write these equations from Eq. (65) of I as

$$[H_{\bar{a}}^{(N-1)} - (\epsilon_a \pm \omega)]y_{\bar{a}\pm} = R_{\bar{a}\pm}\,, \tag{A1}$$

where $H_{\bar{a}}^{(N-1)}$ is the single-channel $V_{jj}^{(N-1)}$ Hamiltonian, and where $R_{\bar{a}\pm}$ contains the RRPA correlation effects.

Before attempting to solve Eq. (A1), one must have DF orbitals available to calculate the potentials in $H_{\bar{a}}^{(N-1)}$ and the interaction terms in $R_{\bar{a}\pm}$. For this purpose, we have a numerical program which calculates the DF orbitals and eigenvalues for closed-shell atoms. The multiconfiguration Dirac-Fock program of Desclaux[45] will serve the same purpose.

As a starting approximation to the solution of Eq. (A1), we take $V_{jj}^{(N-1)}$ orbitals $y_{\bar{a}}^0$, which are solutions, regular at $r = 0$, to the homogeneous $V_{jj}^{(N-1)}$ equations

$$(H_{\bar{a}}^{(N-1)} - E)y_{\bar{a}} = 0\,, \tag{A2}$$

with $E = \epsilon_a \pm \omega$. The solutions to Eq. (A2) for open channels ($E = \epsilon_a + \omega > m$) are normalized to have the asymptotic form

$$y_{\bar{a}}^0(r) \to \begin{pmatrix} ((E+m)/\pi p)^{1/2}\cos X \\ ((E-m)/\pi p)^{1/2}\sin X \end{pmatrix}, \tag{A3}$$

where

$$X = pr + \nu \ln 2pr - (l_{\bar{a}} + 1)\pi/2 + \sigma_{\bar{a}} + \delta_{\bar{a}}\,. \tag{A4}$$

In Eqs. (A3) and (A4) the notation is as in I with $\sigma_{\bar{a}}$ being the Coulomb phase shift and $\delta_{\bar{a}}$ the phase shift due to the short-range part of $V_{jj}^{(N-1)}$. Standard numerical techniques are used to solve Eq. (A2). The equation is integrated outward, using an Adam's-type predict-correct scheme. The equation is then integrated inward using the same scheme from a "practical infinity" starting with asymptotic Dirac-Coulomb wave functions. From the Wronskian of the inward and outward solutions, one determines the phase shift $\delta_{\bar{a}}$ and the normalization constant to give the required asymptotic behavior.

In a lowest approximation we take $y_{\bar{a}}^0$ to represent the solutions to the RRPA equations for open channels, and we ignore the contributions from closed channels and those from negative-frequency orbitals. As mentioned in I, the resulting $V_{jj}^{(N-1)}$ approximation is not usually realistic since the RRPA orbitals are, in fact, more nearly LS coupled than jj coupled for the outer shells of the rare gases. Nevertheless, the $V_{jj}^{(N-1)}$ solution is an entirely adequate first approximation on which to base an iteration solution to the RRPA Eq. (A1).

For convenience, we label each channel by an index i, where $i = (a, \bar{a})$ represents the channel with a hole in state a and a photoelectron in state $\bar{a}$. We let P represent the family of open channels and Q the family of closed channels, and denote the number of channels in P and Q by N_p and N_Q, respectively. Our lowest approximation for the orbitals corresponding to the jth open channel is written

$$\begin{Bmatrix} y_{i+}^{(j)} \simeq y_i^0\delta_{ij} & i \in P \\ y_{i+}^{(j)} \simeq 0 & i \in Q \\ y_{i-}^{(j)} \simeq 0 & \text{all } i \end{Bmatrix}. \tag{A5}$$

The index i ranges over all orbitals including those associated with both open and closed channels.

We can construct a mathematically exact coupled-channel solution to the truncated RRPA Eq. (A1) which reduces to the approximate single-channel solution given in Eq. (A5) when the correlation effects represented by the terms $R_{a\pm}$ are neglected. To obtain this mathematical solution we first construct the radial Green's function associated with the $V_{jj}^{(N-1)}$ approximation. To this end we let $y_i^\infty(r)$ be a solution to the homogeneous equation (A2) singular at $r=0$ and normalized to behave asymptotically as

$$y_i^\infty(r) \to \begin{bmatrix} -((E+m)/\pi p)^{1/2}\sin X \\ ((E-m)/\pi p)^{1/2}\cos X \end{bmatrix} i \in P. \tag{A6}$$

The Wronskian is given by

$$W(y_i^0, y_i^\infty) = 1/\pi, \tag{A7}$$

and the radial Green's function can be written

$$G(r,r') = \pi y_i^0(r_<) y_i^\infty(r_>), \tag{A8}$$

where $r_<$ ($r_>$) is the minimum (maximum) of r and r'. The solution to Eq. (A1) regular at the origin which reduces to $y_i^0(r)$ when the correlation terms $R_{i\pm}(r)$ on the right-hand side of Eq. (A1) is omitted may be written

$$y_{i+}^{(j)} = y_i^0(r)\delta_{ij} + \int_0^\infty G_{i+}(r,r')R_{i+}(r')\,dr', \quad i \in P. \tag{A9}$$

A similar radial Green's function can be introduced for closed channels and for negative-frequency orbitals. In these cases the solutions to Eq. (A2), regular at the origin $y_{i\pm}^0(r)$, grow exponentially at large r, while the solutions which are exponentially damped at large r, $y_{i\pm}^\infty(r)$, are singular at $r=0$. If we let

$$W_\pm = W(y_{i\pm}^0, y_{i\pm}^\infty) \tag{A10}$$

designate the Wronskians of two such independent solutions, then

$$G_{i\pm}(r,r') = (1/W_\pm) y_{i\pm}^0(r_<) y_{i\pm}^\infty(r_>) \tag{A11}$$

and the required Green's functions, and the corresponding solutions to Eq. (A1) are

$$\left.\begin{aligned} y_{i+}^{(j)}(r) &= \int_0^\infty G_{i+}(r,r')R_{i+}(r')\,dr', \quad i \in Q \\ y_{i-}^{(j)}(r) &= \int_0^\infty G_{i-}(r,r')R_{i-}(r')\,dr', \quad \text{all } i \end{aligned}\right\}. \tag{A12}$$

At large r, the solutions given in Eqs. (A12) vanish exponentially. Equations (A9) and (A12) taken together provide a family of N_p independent solutions to the RRPA equations, where N_p is the number of open channels.

To obtain one of these coupled-channel solutions numerically, we start with the approximate single-channel solution given in Eq. (A5) and calculate the correlation terms $R_{i+}(r)$ on the right-hand sides of Eq. (A1) using the lowest approximation. We then use Eqs. (A9) and (A12) to obtain a next approximation for $y_{i+}(r)$ and integrate until the solution converges to a satisfactory limit. In carrying out the iteration, it is convenient to ignore the negative-frequency orbitals $y_{i-}(r)$ entirely at the first stages. The iteration procedure then converges to the $V_{IC}^{(N-1)}$ intermediate-coupling solutions discussed in I. We often find that the $V_{IC}^{(N-1)}$ solutions are accurate approximations to the final RRPA orbitals. The iteration is extended beyond the $V_{IC}^{(N-1)}$ approximation by including the negative-frequency terms in Eq. (A12) and continuing the iteration until final convergence is achieved.

Once a solution to Eq. (A1) is reached, one finds from Eq. (A9) the asymptotic expressions

$$y_i^{(j)}(r) \to y_i^0(r)\delta_{ij} + y_i^\infty(r)\bar{K}_{ij}, \quad \text{for } i,j \in P, \tag{A13}$$

where we have shortened the notation by omitting the subscript + for the open channels on the left-hand side of Eq. (A13). All of the remaining (closed-channel and negative-frequency) orbitals, of course, vanish exponentially. The matrix $\bar{K} = (\bar{K}_{ij})$ is found from Eq. (A9) to be

$$\bar{K}_{ij} = \pi \int_0^\infty y_i^0(r)R_i(r)\,dr, \tag{A14}$$

where R_i is calculated using the solution for channel j.

To transform Eq. (A13) to the form required for the analysis given in Sec. IV C of I, we make use of the relation between the asymptotic $V_{jj}^{(N-1)}$ orbitals of Eqs. (A3) and (A6) and the corresponding Dirac-Coulomb functions f_i and g_i of Eqs. (74) and (75) in I. We find that for large r,

$$\begin{aligned} y_i^0(r) &\to \cos\delta_i f_i(r) + \sin\delta_i g_i(r), \\ y_i^\infty(r) &\to -\sin\delta_i f_i(r) + \cos\delta_i g_i(r), \end{aligned} \tag{A15}$$

where δ_i are the short-range $V_{jj}^{(N-1)}$ phase shifts. By considering the linear combination of mathematical solutions

$$z_i^{(I)}(r) = \sum_j y_i^{(j)}(r)A_{jI}, \tag{A16}$$

we can construct solutions to Eq. (A1) which have the asymptotic form required in I. For this purpose, let us introduce the diagonal $N_p \times N_p$ matrices

$$\begin{aligned} C &= \mathrm{diag}[\cos(\delta_i)], \\ S &= \mathrm{diag}[\sin(\delta_i)]. \end{aligned} \tag{A17}$$

By choosing the matrix $A = (A_{jI})$ to be

$$A = (C - S\bar{K})^{-1}, \tag{A18}$$

and by defining the matrix K as

$$K = (S + C\bar{K})(C - S\bar{K})^{-1}, \tag{A19}$$

we find at large r

$$z_i^{(I)}(r) \rightarrow f_i(r)\delta_{iI} + g_i(r)K_{iI}. \tag{A20}$$

Equation (A20) is precisely the asymptotic condition in terms of Dirac-Coulomb orbitals required for the eigenchannel analysis described in Sec. IV C of I.

We have written a computer program to construct the numerical Green's functions, and starting with the $V_{jj}^{(N-1)}$ solution $y_i^0(r)$ to carry out the iteration solution described above. From the output of this program reduced matrix elements of the dipole transition operator can be calculated and the cross section and angular distribution parameters can be easily obtained.

[1] J. A. R. Samson in *Handbuch der Physik*, Vol. 31, edited by W. Mehlhorn (Springer-Verlag, Berlin, to be published).
[2] A. F. Starace, same as Ref. 1.
[3] M. Ya Amusia and N. A. Cherepkov, Case Stud. At. Phys. 5, 47 (1975); M. Ya Amusia, *Vacuum Ultraviolet Radiation Physics*, edited by E. E. Koch, R. Haensel, and C. Kunz (Pergamon, Braunschweig, 1974), p. 205.
[4] G. Wendin, Ref. 3, p. 225.
[5] W. R. Johnson and K. T. Cheng, Phys. Rev. Lett. 40, 1167 (1978).
[6] W. R. Johnson and V. Radojević, J. Phys. B 11, L773 (1978).
[7] W. R. Johnson and C. D. Lin, Phys. Rev. A 19, 964 (1979) (preceding paper).
[8] H. P. Kelly and R. L. Simons, Phys. Rev. Lett. 30, 529 (1973).
[9] T. N. Chang, Phys. Rev. A 15, 2392 (1977).
[10] T. N. Chang, Phys. Rev. A 18, 1448 (1978).
[11] P. G. Burke and K. T. Taylor, J. Phys. B 8, 2620 (1975).
[12] D. J. Kennedy and S. T. Manson, Phys. Rev. A 5, 227 (1972).
[13] G. V. Marr and J. B. West, At. Data Nucl. Data Tables 18, 497 (1976).
[14] J. B. West and J. Morton, At. Data Nucl. Data Tables 22, 103 (1978).
[15] J. A. R. Samson, Adv. At. Mol. Phys. 2, 177 (1966); (private communication).
[16] W. S. Watson, J. Phys. B 5, 2292 (1972).
[17] J. R. Swanson and L. Armstrong, Jr., Phys. Rev. A 16, 1117 (1977).
[18] J. J. Chang, J. Phys. B 10, 3195 (1977).
[19] R. P. Madden, D. L. Ederer, and K. Codling, Phys. Rev. 177, 136 (1969); K. Codling, R. P. Madden, and D. L. Ederer, Phys. Rev. 155, 26 (1967).
[20] D. L. Moores, Proc. Phys. Soc. 88, 843 (1966); J. Dubau and J. Wells, J. Phys. B 6, 1452 (1973); U. Fano, J. Opt. Soc. Am. 65, 979 (1975).
[21] M. Y. Adam, F. Wuilleumier, N. Sandner, S. Krummacher, V. Schmidt, and W. Mehlhorn, Jpn. J. Appl. Phys. Suppl. 17, (2) 170 (1978).
[22] F. Wuilleumier and M. O. Krause, J. Electron Spectrosc. 15, 15 (1979).
[23] C. D. Lin, Phys. Rev. A 9, 171 (1974).
[24] K. H. Tan and C. E. Brion, J. Electron Spectrosc. 13, 77 (1978).
[25] M. Y. Adam, F. Wuilleumier, S. Krummacher, N. Sandner, V. Schmidt, and W. Mehlhorn, J. Electron Spectrosc. 15, 211 (1979).
[26] J. A. R. Samson and J. L. Gardner, Phys. Rev. Lett. 33, 671 (1974).
[27] T. Gustafsson, Chem. Phys. Lett. 51, 383 (1977).
[28] U. Fano and J. W. Cooper, Rev. Mod. Phys. 40, 441 (1968).
[29] T. E. H. Walker and J. T. Waber, J. Phys. B 7, 674 (1974).
[30] J. A. R. Samson, J. L. Gardner, and A. F. Starace, Phys. Rev. A 12, 1459 (1975).
[31] F. Wuilleumier, M. Y. Adam. P. Dhez, N. Sandner, V. Schmidt, and W. Mehlhorn, Phys. Rev. A 16, 646 (1977).
[32] W. Ong and S. T. Manson, J. Phys. B 11, L163 (1978).
[33] K. T. Taylor, J. Phys. B 10, L699 (1977).
[34] K. Codling, R. G. Houlgate, J. B. West, and P. R. Woodruff, J. Phys. B 9, L83 (1976).
[35] J. L. Dehmer, W. A. Chupka, J. Berkowitz, and W. T. Jivery, Phys. Rev. A 12, 1966 (1975).
[36] F. Wuilleumier and M. O. Krause, Phys. Rev. A 10, 242 (1974).
[37] R. G. Houlgate, J. B. West. K. Codling, and G. V. Marr, J. Electron Spectrosc. 9, 205 (1976).
[38] D. L. Miller, J. D. Dow, R. G. Houlgate, G. V. Marr, and J. B. West, J. Phys. B 10, 3205 (1977).
[39] K. N. Huang and A. F. Starace (private communication).
[40] N. A. Cherepkov, Phys. Lett. 66A, 204 (1978).
[41] J. L. Dehmer and D. Dill, Phys. Rev. Lett. 37, 1049 (1976).
[42] A discussion of the K matrix and related theories can be found in Ref. 2 in the section "Multichannel Quantum Defect Theory."
[43] W. R. Johnson and K. T. Cheng, J. Phys. B 12, 863 (1979).
[44] C. M. Lee, Phys. Rev. A 10, 584 (1974).
[45] J. P. Desclaux, Comput. Phys. Commun. 9, 31 (1975).